



One-pot synthesis of porous silica-supported ultrafine Ni nanoparticles as efficient and stable catalyst for selective hydrogenation of benzophenone

Xianliang Qiao^a, Tiantian She^a, Huiling Zhang^a, Xin Wen^a, Libo Niu^a, Luis Ricardez-Sandoval^b, Jingde Li^{c,*}, Guoyi Bai^{a,*}

^a Key Laboratory of Chemical Biology of Hebei Province, College of Chemistry and Environmental Science, Hebei University, Baoding, 071002, PR China

^b Department of Chemical Engineering, University of Waterloo, Waterloo, ON, N2L 3G1, Canada

^c National-Local Joint Engineering Laboratory for Energy Conservation of Chemical Process Integration and Resources Utilization, Tianjin Key Laboratory of Chemical Process Safety, School of Chemical Engineering and Technology, Hebei University of Technology, Tianjin, 300130, PR China

ARTICLE INFO

Keywords:

Alginate hydrogel
Ni nanoparticles
Benzophenone hydrogenation
High selectivity
Stability

ABSTRACT

In this work, we report a silica-supported ultrafine Ni catalyst for the selective hydrogenation of benzophenone. This material was developed by a facile one-pot co-assembly syntheses strategy, using Ni(II) chelated alginate hydrogel as metal precursor and sacrificial template. Due to the highly active and uniformly dispersed Ni nanoparticles (NPs), 99.8% of benzophenone conversion was achieved. Remarkably, it also reached a 97.7% of selectivity for benzhydrol during benzophenone hydrogenation. Temperature-programmed desorption of ammonia (NH₃-TPD) and Density Functional Theory (DFT) results reveal that the *in-situ* generated sodium carbonate (Na₂CO₃) derived from sodium alginate is essential in tuning the selectivity of benzhydrol: the existence of Na₂CO₃ reduces the surface acidity of catalyst and promotes the desorption of intermediate benzhydrol, preventing its further hydrogenolysis on the surface acidic sites of catalyst. Moreover, the supported Ni catalyst shows no significant loss of its activity during 20 times of recycling.

1. Introduction

Due to the importance as intermediates in drugs and fine chemicals, the selective hydrogenation of aromatic carbonyl compounds towards desirable and valuable products has attracted extensive attentions in the chemical and pharmaceutical industry [1–8]. Many transition-metal catalysts have been developed to facilitate their hydrogenation reactions. However, there are always some by-products obtained in the reactions, leading to a low selectivity to the targeting product [9–11]. Thus, the development of effective catalysts with enhanced hydrogenation selectivity of aromatic carbonyl compounds is still an active and challenging area of research. The reported strategies of improving the selectivity includes: i) modifying the active metal or use bimetallic catalysts [12–14]; ii) developing a suitable support [15–17]; and iii) adding acid or base additives into the reactant, although this may cause a new challenge with the purification of products [18,19].

In the present study, we focus on the development of an efficient catalyst for the selective hydrogenation of benzophenone to benzhydrol. The latter is an important intermediate, which is widely used in the synthesis of benzotropine and diphenhydramine [20–23]. This work is motivated by the fact that most of the catalysts used in such

hydrogenation reaction are noble metals, and their high price and scarcity limit their applications. Therefore, the development of non-precious metal catalysts is attractive. For example, Raney Ni has been reported highly active for benzophenone hydrogenation [24]. However, its pyrophoric nature and the use of strong base in the preparation process limit its further application. Recently, we have also developed several Ni-B amorphous alloy-based catalysts for the hydrogenation of benzophenone with good activity and selectivity properties [25,26]. The stability and selectivity of the Ni-based catalysts, however, still needs to be further improved.

Supported catalysts with highly dispersed and small sized active species would be ideal to design active and stable heterogeneous catalysts [27–29]. The uniform dispersion and small-sized metal NPs usually offers a high catalytic activity. Meanwhile, the synergistic interaction between the active metal species and supports prevents the growth or agglomeration of the metal particles during catalytic reactions, and therefore would result in a good stability [30–33]. However, the controllable preparation of supported ultrafine catalysts is very challenging [34,35]. On the other hand, natural polysaccharide hydrogels have attracted considerable attention because of their environmental sustainability and adjustable functionality. Functionalized

* Corresponding authors.

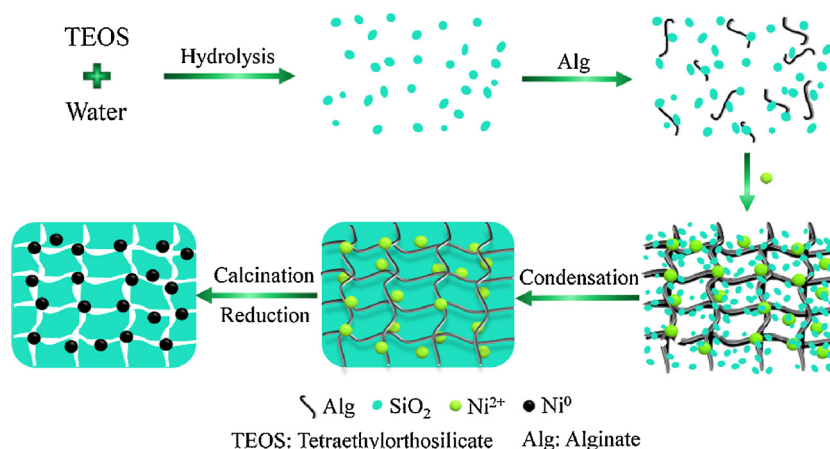
E-mail addresses: jingdeli@hebut.edu.cn (J. Li), baiguoyi@hotmail.com (G. Bai).

<https://doi.org/10.1016/j.apcatb.2019.118111>

Received 15 February 2019; Received in revised form 13 August 2019; Accepted 21 August 2019

Available online 22 August 2019

0926-3373/ © 2019 Elsevier B.V. All rights reserved.



Scheme 1. Schematic illustrating the preparation of Ni@pSiO₂-Alg.

hydrogel has been demonstrated to be a suitable green medium for the uniform immobilization of metal particles [36,37]. In our previous study, we have successfully prepared ultrafine Ni catalyst by using Ni (II) chelated alginate hydrogel as metal precursors [33]. The Ni catalyst showed highly efficient activity in the hydrogenation of unsaturated substrates because of the small and uniformly dispersed Ni NPs. In the research of supported metal catalysts, however, there was still no report on the one-pot synthesis of porous solid oxide supported metal catalysts using active metal ions chelated polysaccharide gel as metal precursor and sacrificial template.

Herein, we demonstrate a straightforward one-pot co-assembly syntheses strategy for SiO₂ supported ultrafine Ni catalyst (denoted as Ni@pSiO₂-Alg, p represents porous, Alg represents alginate, Scheme 1) using Ni(II) chelated natural alginate gels as metal precursors and sacrificial templates. Due to the unique preparation method, the SiO₂ support was developed into a porous structure; consequently, in addition to the ultrafine Ni particles, the resulting high surface area of the SiO₂ support and active metal loading would further benefit the catalytic activity. This represents the other major contribution of this work in the development of active and stable hydrogenation catalysts. The resulting Ni@pSiO₂-Alg catalyst delivers a 99.8% of benzophenone conversion with 97.7% selectivity for benzhydrol during the hydrogenation reaction. The catalyst can still maintain a conversion over 94% for up to 20 times of recycling. The increased selectivity for benzhydrol production was investigated by a combined experimental and theoretical Density Functional Theory (DFT) analysis.

2. Experimental section

2.1. Chemicals and reagents

All chemicals were purchased from Baoding Huaxin Reagent and Apparatus Co., Ltd unless otherwise stated. Ultrapure Ar (99.999%), He (99.999%), 10 vol% H₂/Ar and 10 vol% NH₃/He were supplied by Baoding Zhuoda Gas Co., Ltd.

2.2. Preparation of catalytic materials

First, a mixture of deionized water (40 mL), tetraethoxysilane (TEOS, 5 mL) and HCl (1 M, 1 mL) was vigorously stirred at 50 °C for 4 h, and then added to a solution composed of sodium alginate (1.5 g) and deionized water (90 mL). Once this process was completed, 30 mL of aqueous solution containing x g Ni(NO₃)₂·6H₂O (x = 0.2223, 0.3705, 0.5162) was dropped very slowly to the above solution until the formation of light-green gels. Subsequently, the gels were dried at 80 °C in a water bath and calcined at 450 °C in air for 4 h at a heating rate of 1.0 °C min⁻¹. The calcined samples were reduced under H₂ flow at

450 °C for 4 h; this sample will be referred to as Ni(a)pSiO₂-Alg, where a is the mass content of Ni being 3.0%, 5.0% or 7.0%.

For the sake of comparison, Ni-SiO₂ was prepared using the same procedure with the absence of sodium alginate. SiO₂-Alg support was synthesized without the addition of nickel salt. Additionally, a catalyst was prepared by the conventional impregnation method [28]. That is, Ni(NO₃)₂·6H₂O was dissolved in deionized water, and then SiO₂-Alg support was added into the solution. The mixture was stirred under ultrasound for 20 min and then dried at 80 °C. The dried sample was calcined at 450 °C in air for 4 h at a heating rate of 1.0 °C min⁻¹ and then reduced under H₂ flow at 450 °C for 4 h, this sample will be referred to as Ni-SiO₂-Alg.

2.3. Catalyst characterization

X-ray diffraction (XRD) patterns were recorded on a Bruker D8-Advance X-ray diffractometer using a Cu Kα radiation source. Brunauer-Emmett-Teller (BET) surface area and pore volume were obtained on a Micromeritics Tristar II 3020 surface area and pore analyzer. Fourier transform infrared spectra (FT-IR) were recorded on a Bruker VERTEX 70 Fourier transform spectrometer using KBr pellets. Transmission electron microscopy (TEM) was carried out on a FEI Tecnai G2 F20 microscope. Inductively coupled plasma-mass spectroscopy (ICP-MS) measurement was performed on an Agilent 7700 spectrometer. NH₃-TPD and H₂ chemisorption were carried out on a Micromeritics AutoChem II 2920 instrument equipped with a thermal conductivity detector. X-ray photoelectron spectroscopy (XPS) analysis was conducted using a PHI 1600 spectrometer using Mg Kα X-ray source for excitation.

2.4. Catalyst activity tests

Hydrogenation of benzophenone was performed as follows: absolute ethanol (50 mL), catalyst (0.5 g) and benzophenone (1.0 g, 5.5 mmol) were successively added into a 100 mL Parr 4598 HPHT stainless steel autoclave equipped with a mechanical stirrer and an electrical heating system. The autoclave was first flushed with H₂ five times, followed by evacuation to displace residual air, and then pressured with H₂ to 2.5 MPa and heated to 120 °C. After that, the reaction was initiated by stirring the reactant mixture vigorously, and allowed to proceed for 1 h. Once this process was completed, the autoclave was allowed to cool down to room temperature and the catalyst was separated by filtration for recycling. The resulting solution was analyzed by an Agilent 7820A gas chromatography (GC). The products were identified using gas chromatography-mass spectroscopy (GC-MS) on an Agilent 5977A spectrometer.

2.5. DFT calculations

The DFT calculations were carried out using the VASP package. The Perdew-Burke-Ernzerhof (PBE) functional was used for the exchange and correlation energy terms. The Na_2CO_3 -free and Na_2CO_3 -covered Ni catalysts were modeled using clean and CO_3^{2-} -pre-covered Ni (111) surfaces, respectively. This surface was modeled using a (7×5) unit cell with four atomic layer slab. The vacuum height is set to 15 Å. The bottom Ni layer was fixed in their bulk positions with a calculated lattice parameter of 3.52 Å, whereas the remaining three layers and the adsorbates were allowed to relax. A plane wave cut off of 400 eV was used. The k-space was sampled using a $2 \times 2 \times 1$ Monkhorst-Pack grid. Structures are fully relaxed until the forces acting on the atoms are smaller than 0.03 eV/Å. More details and references are available in the Supplementary Material.

3. Results and discussion

3.1. Characterization of materials

A series of characterization techniques were carried out to investigate the prepared catalysts. The Ni loading, Na content, BET surface area and H_2 -chemisorptions of the catalysts were measured and summarized in Table 1. The results show that the Ni loadings on the SiO_2 support are similar to their corresponding feed values, and the Na contents in the one-pot prepared Ni(a)@p SiO_2 -Alg catalysts (about 8 wt %) are a little higher than that (7.14 wt %) of the two-step impregnation prepared Ni- SiO_2 -Alg catalyst. Among the Ni(a)@p SiO_2 -Alg catalysts, Ni(3%)@p SiO_2 -Alg shows the highest BET surface area ($130 \text{ m}^2 \text{ g}^{-1}$), which decreases gradually with the increase of Ni loading ($a > 3$). Note that, Ni(7%)@p SiO_2 -Alg has higher BET surface area ($76 \text{ m}^2 \text{ g}^{-1}$) than that of Ni(7%)- SiO_2 ($45 \text{ m}^2 \text{ g}^{-1}$). This result is expected and can be attributed to porous structure of Ni(7%)@p SiO_2 -Alg formed by using alginate gels as sacrificial template. Furthermore, among the catalysts studied, Ni(7%)@p SiO_2 -Alg shows the highest H_2 -chemisorption value, which would be an indicative for its high catalytic hydrogenation activity.

Fig. 1 shows the nitrogen adsorption-desorption isotherm and pore size distribution curve of the as-prepared samples. All samples but Ni(7%)- SiO_2 exhibit typical IV isotherm with a typical H3-type hysteresis loop ($P/P_0 > 0.4$). The pore size distribution curves of these samples present sharp peaks at around 3–4 nm, indicating the successful formation of mesoporous structures [38]. The inner graphs of Fig. 1 also show that there are slight decreases in pore size with the increase of Ni loadings for the Ni(a)@p SiO_2 -Alg catalysts. This can be resulted from the blockage of porous channels by Ni NPs as the Ni loading increases [39]; this observation is also in good agreement with the BET results. The Ni(7%)- SiO_2 reveals a type-I isotherm with no hysteresis loop, and there is no obvious peak in its pore size distribution curve, thus highlighting the importance of chelated alginate hydrogel in the formation of porous SiO_2 support.

The XRD patterns of the as-developed samples are shown in Fig. 2. The broad peak at around $2\theta = 23^\circ$ indicates the formation of amorphous silica. In all samples, except Ni(7%)- SiO_2 , the characteristic

diffraction peaks of Na_2CO_3 (30.2° , 35.2° and 38.1°) and NaCl (31.7° and 45.4°) were observed (Fig. 2a). The Na_2CO_3 should be derived from the calcination of sodium alginate [40–42]. To verify this argument, pure sodium alginate powders was calcined at 450°C and the resulting product shows the same characteristic diffraction peaks as Na_2CO_3 (Fig. 2b). Interestingly, there are no apparent XRD diffraction peaks of Ni crystal in all the catalysts prepared by the one-pot co-assembly method, indicating the formation of ultrasmall or highly-dispersed Ni particles. On the other hand, three characteristic peaks at 44.5° , 51.8° and 76.4° related to metallic Ni are detected in Ni(7%)- SiO_2 -Alg. This suggests that supported Ni NPs prepared by the two-step impregnation method show a larger particle size or poorer particle dispersion than that by the one-pot co-assembly method.

FT-IR spectra of sodium alginate, SiO_2 -Alg, Ni(7%)@p SiO_2 -Alg, Ni(7%)- SiO_2 -Alg and Ni(7%)- SiO_2 are presented in Fig. S1. In the spectrum of sodium alginate (a), the peak at about 3340 cm^{-1} is assigned to the stretching vibrations of O–H, and the weak absorption bands at about 2930 cm^{-1} is attributed to the stretching vibrations of C–H. The peaks at about 1620 and 1417 cm^{-1} are associated with the stretching vibrations of carboxyl groups; while the two absorption bands at about 1093 and 1030 cm^{-1} belong to the C–O–C groups of the saccharide structure [43]. The absorption peaks at 1089 , 800 and 466 cm^{-1} in SiO_2 -Alg (b), Ni(7%)@p SiO_2 -Alg (c) and Ni(7%)- SiO_2 -Alg (d) belong to the asymmetric, symmetric stretching and bending vibrations of Si–O–Si, respectively [44]. No absorption peaks of sodium alginate are detected in the above samples. This is similar with that of Ni(7%)- SiO_2 (e), for which no sodium alginate was introduced during its preparation. These observations confirm the successful removal of sodium alginate in the as-prepared catalysts.

H_2 -TPR is used to explore the reduction behavior of these as-developed catalysts. As shown in Fig. 3a, the peaks at lower temperatures can be assigned to the reduction of bulk Ni oxides which interact weakly with SiO_2 , whereas the peaks at higher temperatures can be ascribed to the reduction of ultrasmall and highly-dispersed Ni particles, which strongly interact with SiO_2 [45,46]. A sharp reduction peak at about 350°C is observed in NiO(7%)- SiO_2 , which suggests the existence of large NiO particles and weak interactions between Ni with SiO_2 after reduction. However, in the case of NiO(3%)@p SiO_2 -Alg, NiO(5%)@p SiO_2 -Alg and NiO(7%)@p SiO_2 -Alg, most of Ni species were reduced at around 500°C , indicating the existence of stronger interactions between Ni and SiO_2 . As compared with that of NiO(7%)@p SiO_2 -Alg, two distinct reduction peaks appear around 350 and 480°C in NiO(7%)- SiO_2 -Alg, together with a very small reduction peak at around 632°C , suggesting a relatively weaker interaction between Ni and SiO_2 . Moreover, the relatively less concentrated reduction peaks of NiO(7%)- SiO_2 -Alg also suggests a poor dispersion of Ni species [47].

Fig. 3b shows XPS spectra of Ni 2p in the reduced Ni(7%)@p SiO_2 -Alg and Ni(7%)- SiO_2 -Alg. For the Ni(7%)@p SiO_2 -Alg, three peaks appear at 852.91, 856.41 and 861.48 eV, respectively. The first peak is ascribed to the metallic Ni, whereas the other two peaks are attributed to NiO and its satellite peak, which is mainly formed by the oxidation of metallic Ni in air before XPS analysis [48,49]. Moreover, Ni(7%)- SiO_2 -Alg also exhibits three peaks at 852.44, 855.64 and 861.16 eV, respectively. The upshift of the Ni 2p peaks of Ni(7%)@p SiO_2 -Alg

Table 1
Physicochemical properties of different samples.

Sample	Ni loadings (wt %) ^a	Na contents (wt %) ^a	Surface area ($\text{m}^2 \text{ g}^{-1}$)	H_2 -chemisorption ($\text{cm}^3 \text{ g}^{-1}$)
SiO_2 -Alg	–	8.35	187	–
Ni(3%)@p SiO_2 -Alg	2.94	7.99	130	0.053
Ni(5%)@p SiO_2 -Alg	5.20	8.32	93	0.068
Ni(7%)@p SiO_2 -Alg	6.88	8.33	76	0.115
Ni(7%)- SiO_2 -Alg	6.79	7.14	47	0.083
Ni(7%)- SiO_2	6.94	–	45	0.098

^a Based on ICP-MS results.

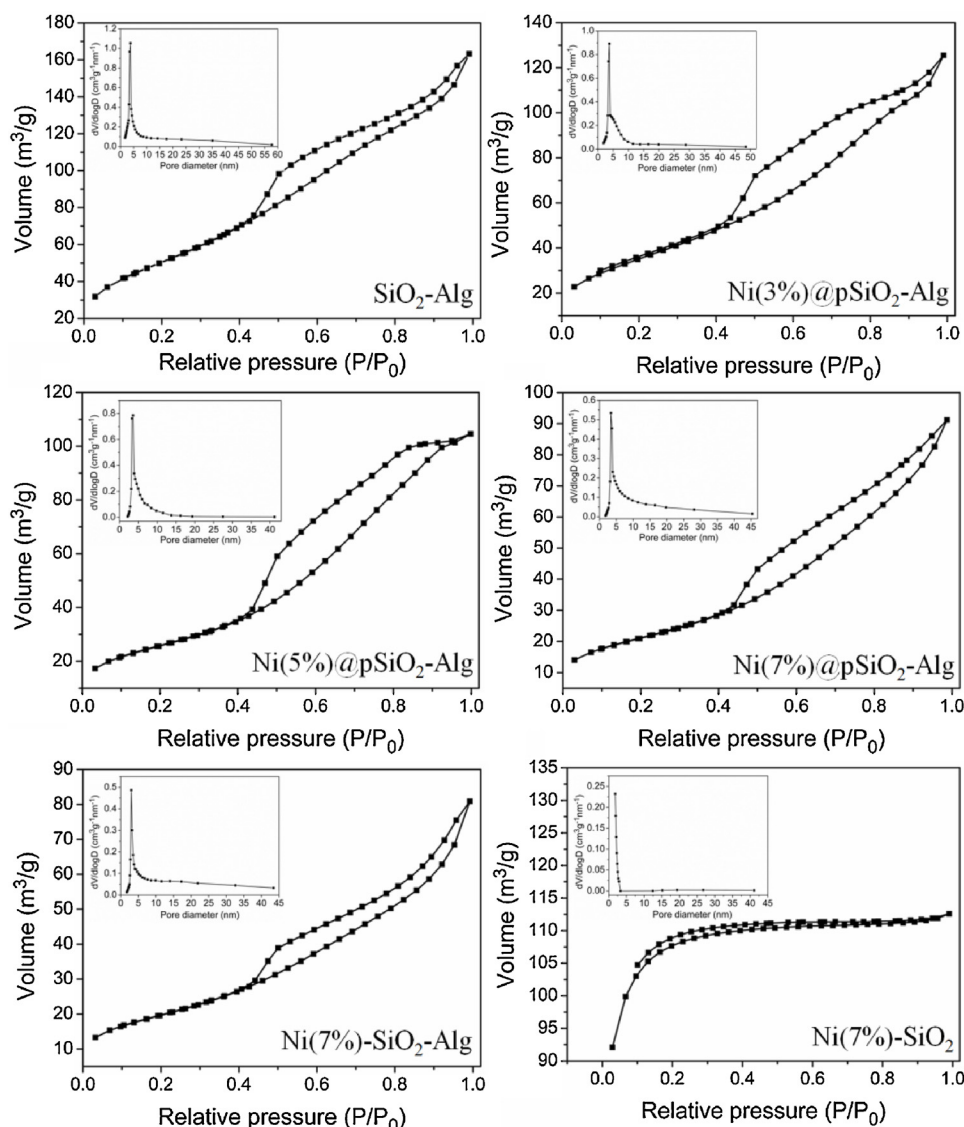


Fig. 1. N_2 adsorption-desorption isotherms and pore size distributions of different samples.

towards high energies usually indicates the existence of a stronger metal-support interaction between Ni and SiO_2 [49,50]. Accordingly, one can expect a good stability performance of Ni(7%)@pSiO₂-Alg because of the enhanced anchoring ability of SiO₂ towards the Ni NPs.

Fig. 4 presents the TEM images and particle size distributions of Ni(7%)@pSiO₂-Alg, Ni(7%)-SiO₂ and Ni(7%)-SiO₂-Alg. It shows that Ni

(7%)@pSiO₂-Alg has a narrow Ni distribution of 3.59 nm with an average size of 5.8 nm (Fig. 4a). This is mainly attributed to the coordination of Ni(II) ions with sodium alginate during preparation, resulting in highly-dispersed and ultrasmall Ni NPs. The high-resolution TEM image of Ni(7%)@pSiO₂-Alg (Fig. 4a, inset) shows clear lattice fringes with a lattice spacing of 0.203 nm, belonging to the d-spacing of

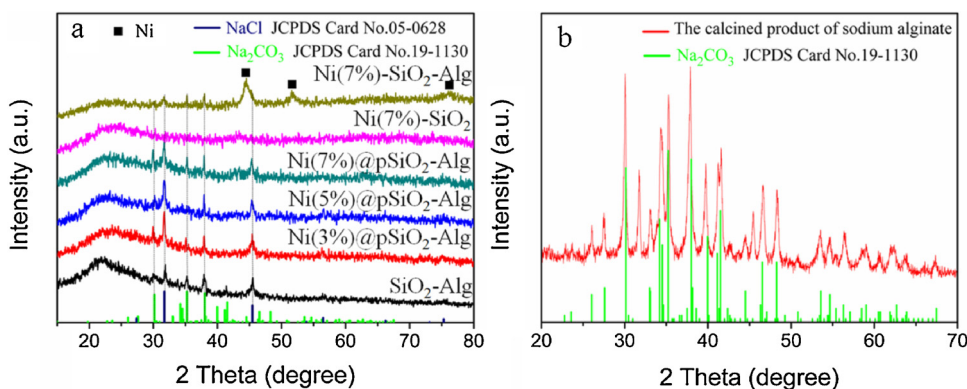


Fig. 2. XRD patterns of the different samples.

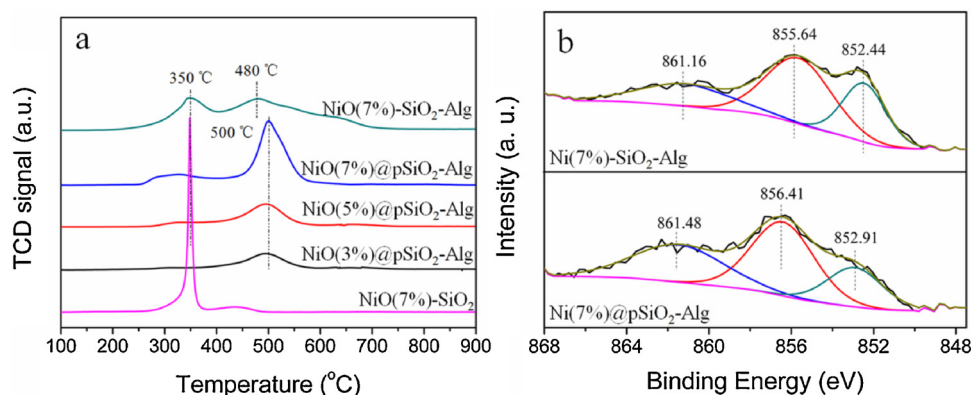


Fig. 3. a) H₂-TPR profiles of calcined samples; b) XPS spectra of Ni 2p in selected catalysts.

the (111) plane in the cubic Ni (JCPDS 87-0712). The Ni(7%)-SiO₂ samples, however, shows large Ni particle sizes (about 12.8 nm) together with certain agglomeration (Fig. 4b). Particularly, Ni(7%)-SiO₂-Alg, prepared by the two-step impregnation method, shows a much wider Ni NPs distribution (11–36 nm) with a large average size of 19.0 nm (Fig. 4c), indicating the poor dispersion and agglomeration of Ni particles in this catalyst. Furthermore, the scanning transmission electron microscope (STEM) and elemental mapping results of Ni(7%)@pSiO₂-Alg further confirms the uniform distribution of the Ni species, as well as Na, Si and O (Fig. 4d).

3.2. Catalytic performances of materials

The catalytic performances of the as-prepared catalysts towards benzophenone hydrogenation were evaluated and reported in Table 2. The results show that, in benzophenone hydrogenation, benzhydrol and diphenylmethane are the main product and byproduct, respectively. For the Ni(a)@pSiO₂-Alg catalysts, the conversion of benzophenone increased with the increase of the Ni loading, and a 99.8% conversion was obtained over Ni(7%)@pSiO₂-Alg. The conversion is much higher than those of Ni(7%)-SiO₂-Alg (65.0%) and Ni(7%)-SiO₂ (78.8%) with the same Ni loadings; this is in good agreement with their corresponding turn over frequency (TOF) values. As discussed before, we ascribe this to the ultrasmall and highly-dispersed Ni NPs of Ni(7%)@pSiO₂-Alg, as well as its porous nature which exposes more active sites for reactants. Remarkably, both Ni(a)@pSiO₂-Alg and Ni(7%)-SiO₂-Alg showed an over 96.0% selectivity for benzhydrol, whereas only 85.9% selectivity for benzhydrol was obtained with Ni(7%)-SiO₂.

3.3. Mechanism insight into the selectivity improvement

According to the XRD results (Fig. 2a), except Ni(7%)-SiO₂, the formation of Na₂CO₃ has been confirmed in Ni(3%)@pSiO₂-Alg, Ni(5%)@pSiO₂-Alg, Ni(7%)@pSiO₂-Alg and Ni(7%)-SiO₂-Alg. Meanwhile, all these alginate derived catalysts deliver much higher selectivity for benzhydrol than Ni(7%)-SiO₂ (Table 2). Therefore, it is reasonable to assume that the *in-situ* generated Na₂CO₃ is the key factor for the enhanced hydrogenation selectivity of benzophenone. To verify this assumption, the acid-base properties of Ni(7%)@pSiO₂-Alg and Ni(7%)-SiO₂ were first examined by NH₃-TPD. Fig. S2 shows that the NH₃ desorption peaks of Ni(7%)@pSiO₂-Alg are much smaller than those of Ni(7%)-SiO₂. Furthermore, the high-temperature desorption peak (569 °C) moves to a lower temperature (518 °C) in Ni(7%)@pSiO₂-Alg as compared with that of Ni(7%)-SiO₂. These results demonstrate that Ni(7%)@pSiO₂-Alg has less acidic sites and lower strong acid strength, which could prevent further hydrogenolysis of benzhydrol on the surface acidic sites of catalyst [51,52].

Next, a washing contrast experiment was carried out to remove Na₂CO₃ in Ni(7%)@pSiO₂-Alg. In brief, the calcined sample NiO(7%)@

pSiO₂-Alg was initially dispersed in a flask containing 50 mL deionized water and stirred for 12 h to dissolve the Na₂CO₃ generated during preparation. Then, the treated sample was dried and reduced under H₂ flow; this sample was denoted as Ni(7%)@pSiO₂-Alg-w. The results of benzophenone hydrogenation over Ni(7%)@pSiO₂-Alg and Ni(7%)@pSiO₂-Alg-w are listed in Table 3. These results show that the selectivity for benzhydrol decreased from 97.7% to 85.7% after washing, together with the selectivity improvement of diphenylmethane from 1.4% to 9.8%. The disappearance of characteristic peaks of Na₂CO₃ in Ni(7%)@pSiO₂-Alg-w indicates the leaching of Na₂CO₃ during washing (Fig. S3). Moreover, the dramatic decrease of Na content in Ni(7%)@pSiO₂-Alg-w (Table 3), and the high pH value (about 11) of the filtrate produced in water-washing process confirms the successful removal of Na₂CO₃ from Ni(7%)@pSiO₂-Alg-w. This is also consistent with the NH₃-TPD analysis, which shows that both of the acidic amount and strength of Ni(7%)@pSiO₂-Alg-w were increased after washing (Fig. S2). On the other hand, certain amount of Na₂CO₃ was added to Ni(7%)-SiO₂, which has an initial low selectivity for benzhydrol, during its preparation process; the obtained sample was referred to as Ni(7%)-SiO₂-Na₂CO₃. The experimental result showed that the selectivity for benzhydrol increased from 85.9% to 98.3% over Ni(7%)-SiO₂-Na₂CO₃, although the conversion of benzophenone was only 77.2% (Table 3). All these observations strongly confirm that the *in-situ* generated Na₂CO₃ species in catalysts is responsible for the improved selectivity for benzhydrol.

To have an in-depth understanding on the enhanced selectivity for benzhydrol in the catalytic hydrogenation of benzophenone over Ni(7%)@pSiO₂-Alg, the adsorption behavior of the surface species and their reaction kinetics on clean and CO₃²⁻-pre-covered Ni (111) were investigated using first-principles DFT calculations (See Supplementary Material for computational details). Note that, to leave enough space for the reacting molecule to interact with the Ni surface, CO₃²⁻ was placed at different surface sites far away from the reacting molecule in the Ni (7 × 5) unit cell. Then, the most stable co-adsorption configuration was determined. Fig. 5a and b shows the proposed reaction pathways on the clean and CO₃²⁻-pre-covered Ni (111) surfaces, respectively, where the same pathways are adopted: i) hydrogenation of benzophenone starts with its adsorption on the Ni catalyst surface; ii) the continuous hydrogenation of benzophenone (R) leads to the formation of four surface species (in the following sequence): “benzophenone + H” (Int1), benzhydrol (P1), “benzhydrol – OH” (Int2), diphenylmethane (P2); iii) the desorption of P1 and P2 result in the production of benzhydrol and diphenylmethane, respectively. The adsorption of the surface species (R, Int1, P1, Int2, P2) was examined (Fig. S4), and the corresponding adsorption energies (E_{ads}) are shown in Table 4. It was found that the adsorption energies of these hydrogenation surface species on CO₃²⁻-pre-covered Ni (111) is much lower than that on clean Ni (111) surface. For example, the adsorption energy of benzhydrol (P1) drops from 1.07 to 0.33 eV when CO₃²⁻ is covered on

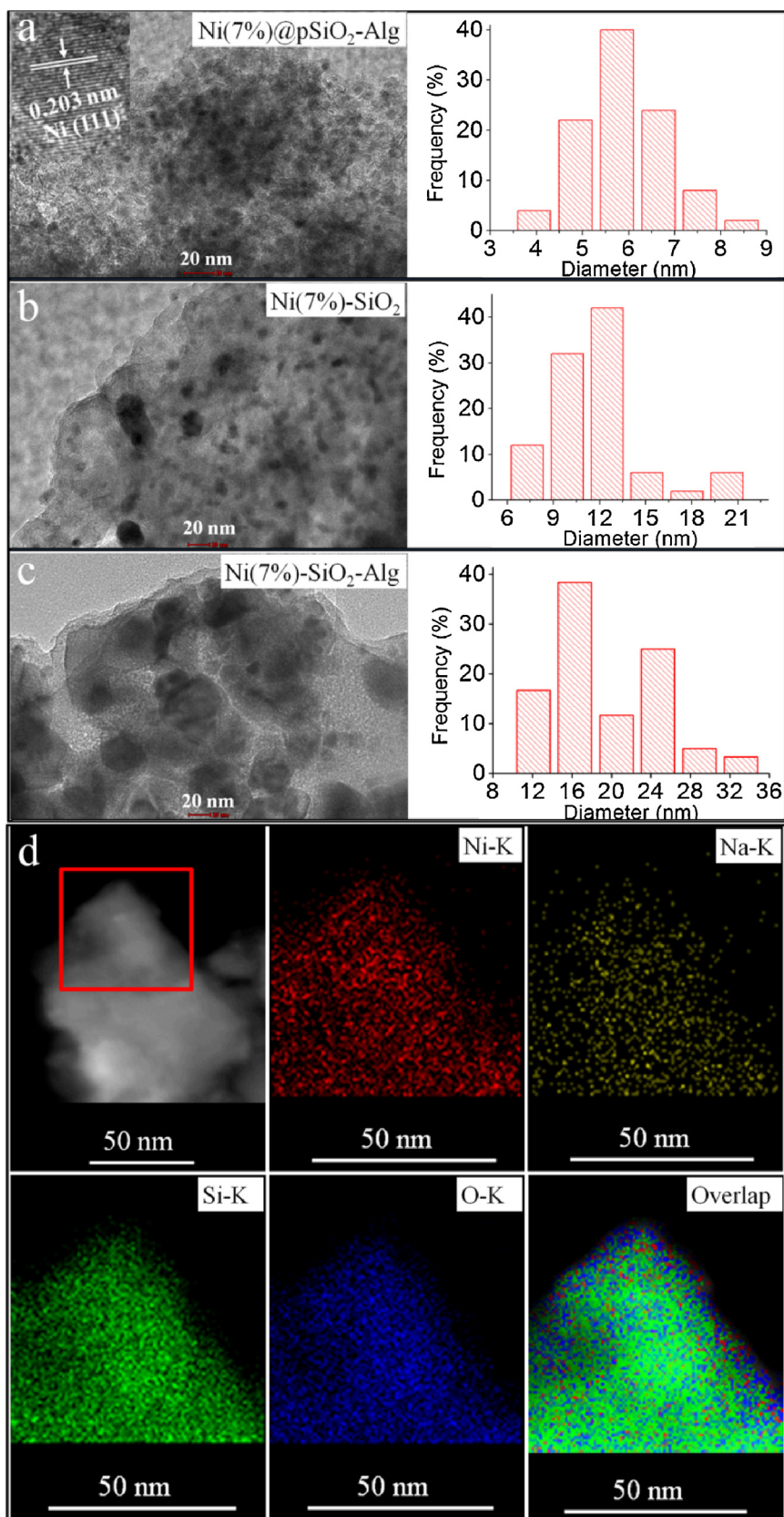


Fig. 4. TEM images and particle size distributions of selected catalysts: a) Ni(7%)@pSiO₂-Alg; b) Ni(7%)-SiO₂; c) Ni(7%)-SiO₂-Alg; HAADF-STEM image: d) Ni(7%)@pSiO₂-Alg, with elemental mapping of Ni, Na, Si, O and their overlap.

Table 2
Catalytic performance of different catalysts for benzophenone hydrogenation.

Entry	Catalysts	Conversion (%) ^a	Selectivity (%)			TOF (10 ³ h ⁻¹) ^b
			benzhydrol	diphenylmethane	others	
1	Ni(3%)/pSiO ₂ -Alg	52.3	97.3	1.8	0.8	1.64
2	Ni(5%)/pSiO ₂ -Alg	62.5	97.4	1.3	1.4	1.59
3	Ni(7%)/pSiO ₂ -Alg	99.8	97.7	1.4	0.9	1.55
4	Ni(7%)-SiO ₂ -Alg	65.0	96.6	1.6	1.8	1.14
5	Ni(7%)-SiO ₂	78.8	85.9	8.3	5.8	1.22

^a Reaction conditions: benzophenone (5.5 mmol), absolute ethanol (50 mL), catalyst (0.5 g), P(H₂) = 2.5 MPa, 400 rpm, 120 °C, 1 h.

^b The TOF values were calculated based on the conversion of benzophenone in 30 min.

Table 3
Na content and catalytic performance of different catalysts.

Catalysts	Na content (wt %)	Conversion (%)	Selectivity (%)		
			benzhydrol	diphenylmethane	others
Ni(7%)/pSiO ₂ -Alg	8.33	99.8	97.7	1.4	0.9
Ni(7%)/pSiO ₂ -Alg-w	1.06	99.8	85.7	9.8	4.5
Ni(7%)-SiO ₂ -Na ₂ CO ₃	3.01	77.2	98.3	0.3	1.4

Reaction conditions: benzophenone (5.5 mmol), absolute ethanol (50 mL), catalyst (0.5 g), P(H₂) = 2.5 MPa, 400 rpm, 120 °C, 1 h.

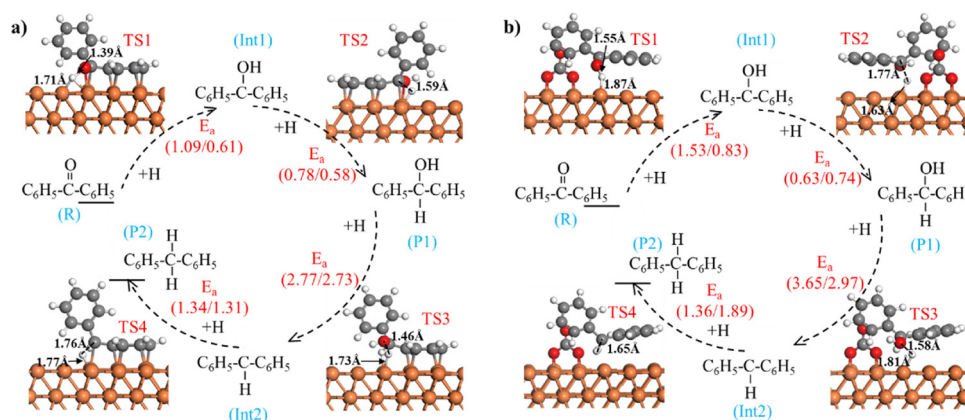


Fig. 5. Geometric structures of the transition state (T.S), and forward/backward activation energies (E_a , eV) of the proposed elementary reactions in benzophenone hydrogenation reaction on a) clean and b) CO_3^{2-} -pre-covered Ni (111) surface models. Orange (Ni), gray (C), red (O), white (H) (For interpretation of the references to colour in this figure legend, the reader is referred to the web version of this article.).

Table 4
The adsorption energies of various surface species or intermediates on clean and CO_3^{2-} -pre-covered Ni (111) surfaces.

Surface species	Ni (111) models	
	clean (E_{ads} , eV)	CO_3^{2-} -pre-covered (E_{ads} , eV)
benzophenone (R)	1.26	0.48
"benzophenone + H" (Int1)	1.53	0.59
benzhydrol (P1)	1.07	0.33
"benzhydrol-OH" (Int2)	2.02	0.64
diphenylmethane (P2)	0.92	0.15

Ni (111) surface. This indicates that the existence of CO_3^{2-} can significantly destabilize benzhydrol on the surface of catalyst and promote benzhydrol desorption on Ni (111) surface. This destabilization effect, combined with the reduced surface acidity caused by Na_2CO_3 (proved by NH_3 -TPD), can prevent benzhydrol from its further hydrogenolysis on the surface of catalyst, and therefore improve the selectivity for benzhydrol. Moreover, the kinetic analysis shows that: i) among the four hydrogenation steps, the hydrogenolysis of benzhydrol (P1) into intermediate species Int2 has the highest energy barrier, suggesting

benzhydrol further hydrogenolysis (P1 to Int2) is the rate-limiting step for the complete hydrogenation of benzophenone (R to P2); ii) the energy barrier for benzhydrol (P1) further hydrogenolysis to Int2 on CO_3^{2-} -pre-covered Ni (111) surface (3.65 eV) is much higher than that on clean Ni (111) surface (2.77 eV), indicating further hydrogenolysis of benzhydrol (P1) is kinetically hindered by the presence of CO_3^{2-} . Therefore, CO_3^{2-} affects the competition between P1 adsorption and hydrogenolysis: in the presence of CO_3^{2-} , the hydrogenolysis barrier is higher whereas desorption presents a low energy barrier and thus it is easier to proceed. This benefits the enhanced benzhydrol selectivity on the Ni(7%)/pSiO₂-Alg catalyst. As discussed above, it might be the high repulsion between CO_3^{2-} and the reacting molecules that leads to the large energy differences between the two catalysts. In fact, in DFT studies, it is not the absolute value in the energy barrier but the trends in changes in the energetics that matters to derive key outcomes from the calculations.

Based on the above experimental and DFT results, therefore, a route for the selective hydrogenation of benzophenone was proposed in Fig. 6. When there was no Na_2CO_3 existed on the surface of the catalyst, the hydrogenolysis of intermediate benzhydrol may proceed to form diphenylmethane. Upon the introduction of sodium alginate, the *in-situ* generated Na_2CO_3 will partially cover the surface of Ni catalyst and

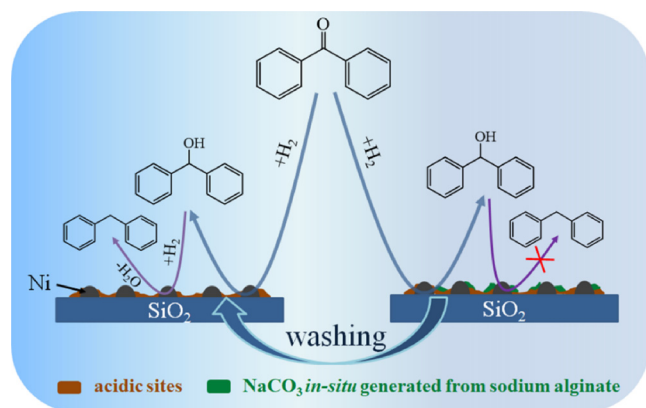


Fig. 6. Proposed route for the hydrogenation of benzophenone.

neutralize some acidic sites, preventing intermediate benzhydrol from further hydrogenolysis to diphenylmethane, and therefore resulting in its increased selectivity. Notably, the critical role of Na_2CO_3 in catalyst can be further confirmed by interesting contrast experiments (Table 3), in which the selectivity for benzhydrol decreased after the Na_2CO_3 in $\text{Ni}(7\%)\text{@pSiO}_2\text{-Alg}$ was removed by washing, or the selectivity for benzhydrol increased after some Na_2CO_3 was added to a poor-selectivity catalyst $\text{Ni}(7\%)\text{-SiO}_2$.

3.4. Reusability of the catalysts

The reusability of $\text{Ni}(7\%)\text{-SiO}_2$, $\text{Ni}(7\%)\text{-SiO}_2\text{-Alg}$, $\text{Ni}(7\%)\text{@pSiO}_2\text{-Alg}$ and $\text{Ni}(7\%)\text{@pSiO}_2\text{-Alg-w}$ were investigated in the hydrogenation of benzophenone (Fig. 7). Among these catalysts, $\text{Ni}(7\%)\text{@pSiO}_2\text{-Alg}$ showed the highest activity and stability in 5 runs (Fig. 7c). Further reusability study revealed that the conversion of benzophenone remained over 94% after 20 times of recycling over $\text{Ni}(7\%)\text{@pSiO}_2\text{-Alg}$ (Fig. S5), which is much better than all previously reported results (Table S1). This can be attributed to the ultrafine and highly-dispersed

Ni NPs, as well as the strong metal-support interaction between Ni NPs and SiO_2 , as evidenced by the TEM, H_2 -TPR and XPS characterizations. Furthermore, a good stability was also obtained over $\text{Ni}(7\%)\text{@pSiO}_2\text{-Alg-w}$ with the conversion of benzophenone keeping over 99% in 5 runs. However, the conversions of benzophenone decreased from 85.9% and 65.0% to below 50% within 5 runs over $\text{Ni}(7\%)\text{-SiO}_2$ and $\text{Ni}(7\%)\text{-SiO}_2\text{-Alg}$, respectively. These observations indicate the poor stabilities of the alginate-free and two-step impregnation catalysts, and therefore highlighting the critical role of the one-pot addition of alginate during catalyst preparation.

4. Conclusions

In summary, a facile one-pot co-assembly method was successfully developed to prepare porous silica-supported ultrafine Ni catalyst for the selective hydrogenation of benzophenone. The key of this preparation method is using Ni(II) chelated alginate gels as metal precursor and sacrificial template. The resulting $\text{Ni@pSiO}_2\text{-Alg}$ catalyst delivers excellent catalytic activity, selectivity and stability in benzophenone hydrogenation. Specifically, a 99.8% of benzophenone conversion was achieved due to the ultrafine and highly-dispersed Ni NPs. Meanwhile, it also reached a 97.7% of selectivity for benzhydrol resulted from the *in-situ* generated Na_2CO_3 on Ni surface during catalyst preparation, which has been confirmed by NH_3 -TPD and DFT calculations. Owing to the simple preparation process, the green nature of sodium alginate, and the excellent catalytic performance of the catalyst, the present study provides an attractive and promising strategy for the design of efficient and stable supported catalysts for hydrogenation reactions.

Declaration of Competing Interest

The authors declare that they have no known competing financial interests or personal relationships that could have appeared to influence the work reported in this paper.

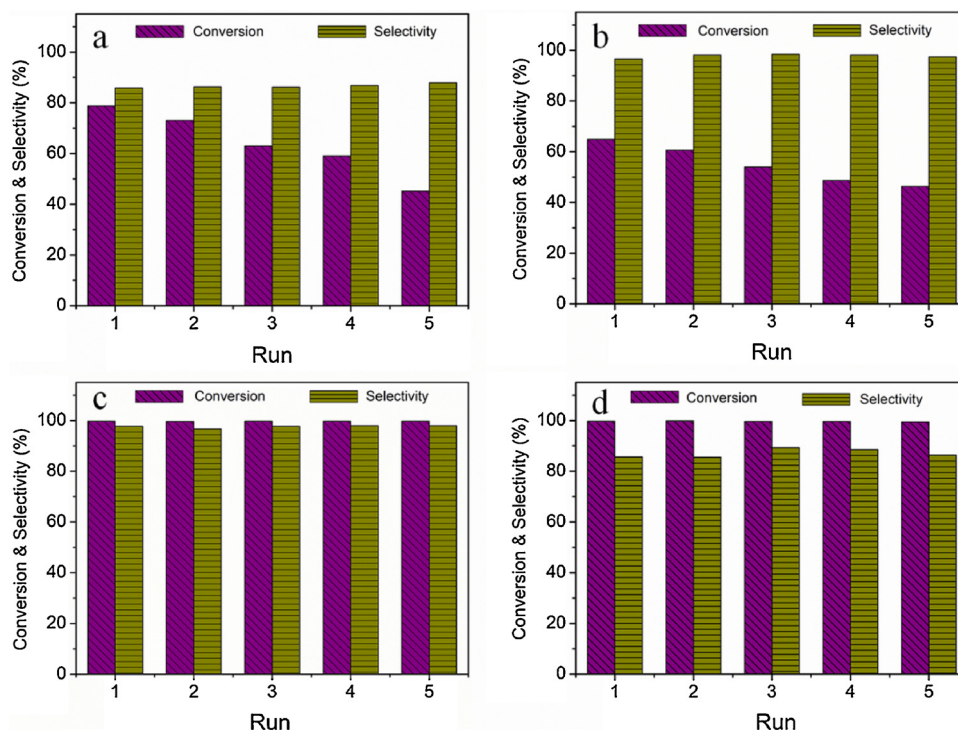


Fig. 7. Reusability results of different catalysts: a) $\text{Ni}(7\%)\text{-SiO}_2$; b) $\text{Ni}(7\%)\text{-SiO}_2\text{-Alg}$; c) $\text{Ni}(7\%)\text{@pSiO}_2\text{-Alg}$; d) $\text{Ni}(7\%)\text{@pSiO}_2\text{-Alg-w}$. Reaction conditions: benzophenone (5.5 mmol), absolute ethanol (50 mL), catalyst (0.5 g), $P(\text{H}_2) = 2.5$ MPa, 400 rpm, 120°C , 1 h.

Acknowledgments

This work was supported by the National Natural Science Foundation of China (21676068 and 21376060), Natural Science Foundation of Hebei Province (B2019201341), hundred outstanding innovative personnel support plan of Hebei Universities (SLRC2017020), 333 talent project of Hebei Province (A2016005006), and Outstanding Young Talents Project of Hebei High Education Institutions (BJ2019013). The authors also gratefully acknowledge the computing facilities of the Shared Hierarchical Academic Research Computing Network (SHARCNET: www.sharcnet.ca) and Compute/Calcul Canada.

Appendix A. Supplementary data

Supplementary data associated with this article can be found, in the online version, at <https://doi.org/10.1016/j.apcatb.2019.118111>.

References

- [1] M. Tang, S. Mao, M. Li, Z. Wei, F. Xu, H. Li, Y. Wang, RuPd alloy nanoparticles supported on N-doped carbon as an efficient and stable catalyst for benzoic acid hydrogenation, *ACS Catal.* 5 (2015) 3100–3107.
- [2] G. Bai, Z. Zhao, H. Dong, L. Niu, Y. Wang, Q. Chen, A NiPd-B-PEG (800) amorphous alloy catalyst for the chemoselective hydrogenation of electron-deficient aromatic substrates, *ChemCatChem*. 6 (2014) 655–662.
- [3] T.M. Townsend, C. Kirby, A. Ruff, A.R. O'Connor, Transfer hydrogenation of aromatic and linear aldehydes catalyzed using Cp* Ir (pyridinesulfonamide) Cl complexes under base-free conditions, *J. Organomet. Chem.* 843 (2017) 7–13.
- [4] J. Li, Z. Lin, Q. Huang, Q. Wang, L. Tang, J. Zhu, J. Deng, Asymmetric transfer hydrogenation of aryl ketoesters with a chiral double-chain surfactant-type catalyst in water, *Green Chem.* 19 (2017) 5367–5370.
- [5] F. Kallmeier, T. Irrgang, T. Dietel, R. Kempe, Highly active and selective manganese C=O bond hydrogenation catalysts: the importance of the multidentate ligand, the ancillary ligands, and the oxidation state, *Angew. Chem. Int. Ed.* 55 (2016) 11806–11809.
- [6] Y. Wei, B. Rao, X. Cong, X. Zeng, Highly selective hydrogenation of aromatic ketones and phenols enabled by cyclic (amino)(alkyl) carbene rhodium complexes, *J. Am. Chem. Soc.* 137 (2015) 9250–9253.
- [7] P. Sudakar, G. Gunasekar, I. Baek, S. Yoon, Recyclable and efficient heterogenized Rh and Ir catalysts for the transfer hydrogenation of carbonyl compounds in aqueous medium, *Green Chem.* 18 (2016) 6456–6461.
- [8] N. Gorgas, B. Stoger, L.F. Veiros, K. Kirchner, Highly efficient and selective hydrogenation of aldehydes: a well-defined Fe(II) catalyst exhibits noble-metal activity, *ACS Catal.* 6 (2016) 2664–2672.
- [9] Y.G. Zhou, Asymmetric hydrogenation of heteroaromatic compounds, *Acc. Chem. Res.* 40 (2007) 1357–1366.
- [10] H.Y. Jiang, X.X. Zheng, Tuning the chemoselective hydrogenation of aromatic ketones, aromatic aldehydes and quinolines catalyzed by phosphine functionalized ionic liquid stabilized ruthenium nanoparticles, *Catal. Sci. Technol.* 5 (2015) 3728–3734.
- [11] J.A. Widegren, R.G. Finke, A review of soluble transition-metal nanoclusters as arene hydrogenation catalysts, *J. Mol. Catal. A Chem.* 191 (2003) 187–207.
- [12] I. Schrader, J. Warneke, J. Backenkohler, S. Kunz, Functionalization of platinum nanoparticles with L-proline: simultaneous enhancements of catalytic activity and selectivity, *J. Am. Chem. Soc.* 137 (2015) 905–912.
- [13] V. Vetere, A.B. Merlo, M.L. Casella, Chemoselective hydrogenation of aromatic ketones with Pt-based heterogeneous catalysts. Substituent effects, *Appl. Catal. A Gen.* 491 (2015) 70–77.
- [14] W.S. Putro, T. Kojima, T. Hara, N. Ichikuni, S. Shimazu, Selective hydrogenation of unsaturated carbonyls by Ni-Fe-based alloy catalysts, *Catal. Sci. Technol.* 7 (2017) 3637–3646.
- [15] Y. Ma, G. Xu, H. Wang, Y. Wang, Y. Zhang, Y. Fu, Cobalt nanocluster supported on ZrReO₄ for the selective hydrogenation of biomass derived aromatic aldehydes and ketones in water, *ACS Catal.* 8 (2018) 1268–1277.
- [16] B. Schimmoeller, F. Hoxha, T. Mallat, F. Krumeich, S.E. Pratsinis, A. Baiker, Fine tuning the surface acid/base properties of single step flame-made Pt/alumina, *Appl. Catal. A Gen.* 374 (2010) 48–57.
- [17] S.K. Wilkinson, I. McManus, H. Daly, J.M. Thompson, C. Hardacre, N. Sedaie Bonab, J. ten Dam, M.J.H. Simmons, C. D'Agostino, J. McGregor, L.F. Gladden, E.H.A. Stitt, Kinetic analysis methodology to elucidate the roles of metal, support and solvent for the hydrogenation of 4-phenyl-2-butanone over Pt/TiO₂, *J. Catal.* 330 (2015) 362–373.
- [18] Y. Li, C. Topf, X. Cui, K. Junge, M. Beller, Lewis acid promoted ruthenium(II)-catalyzed etherifications by selective hydrogenation of carboxylic acids/esters, *Angew. Chem. Int. Ed.* 127 (2015) 5285–5289.
- [19] X. Wen, Y. Cao, X. Qiao, L. Niu, L. Huo, G. Bai, Significant effect of base on the improvement of selectivity in the hydrogenation of benzoic acid over NiZrB amorphous alloy supported on γ -Al₂O₃, *Catal. Sci. Technol.* 5 (2015) 3281–3287.
- [20] M. Villalba, M. del Pozo, E.J. Calvo, Electrocatalytic hydrogenation of acetophenone and benzophenone using palladium electrodes, *Electrochim. Acta* 164 (2015) 125–131.
- [21] K.Y. Wan, M.M.H. Sung, A.J. Lough, R.H. Morris, Half-sandwich ruthenium catalyst bearing an enantiopure primary amine tethered to an N-heterocyclic carbene for ketone hydrogenation, *ACS Catal.* 7 (2017) 6827–6842.
- [22] C.M. Cirtiu, A. Brisch-Wittmeyer, H. Ménard, Comparative study of catalytic and electrocatalytic hydrogenation of benzophenone, *Catal. Commun.* 8 (2007) 751–754.
- [23] G.F. Santori, A.G. Moglioni, V. Vetere, G.Y.M. Iglesias, M.L. Casella, O.A. Ferretti, Hydrogenation of aromatic ketones with Pt- and Sn-modified Pt catalysts, *Appl. Catal. A Gen.* 269 (2004) 215–223.
- [24] S.P. Bawane, S.B. Sawant, Kinetics of liquid-phase catalytic hydrogenation of benzophenone to benzhydrol, *Org. Process Res. Dev.* 7 (2003) 769–773.
- [25] G. Bai, L. Niu, M. Qiu, F. He, X. Fan, H. Dou, X. Zhang, Liquid-phase selective hydrogenation of benzophenone over ultrasonic-assisted Ni-La-B amorphous alloy catalyst, *Catal. Commun.* 12 (2010) 212–216.
- [26] G. Bai, Z. Zhao, L. Niu, H. Dong, M. Qiu, F. Li, Q. Chen, G. Chen, Effect of polymers and alkaline earth metals on the catalytic performance of Ni-B amorphous alloy in benzophenone hydrogenation, *Catal. Commun.* 23 (2012) 34–38.
- [27] S. Zhang, C.R. Chang, Z.Q. Huang, J. Li, Z. Wu, Y. Ma, Z. Zhang, Y. Wang, Y. Qu, High catalytic activity and chemoselectivity of sub-nanometric Pd clusters on porous nanorods of CeO₂ for hydrogenation of nitroarenes, *J. Am. Chem. Soc.* 138 (2016) 2629–2637.
- [28] X. Kang, H. Liu, M. Hou, X. Sun, H. Han, T. Jiang, Z. Zhang, B. Han, Synthesis of supported ultrafine non-noble subnanometer-scale metal particles derived from metal-organic frameworks as highly efficient heterogeneous catalysts, *Angew. Chem. Int. Ed.* 55 (2016) 1080–1084.
- [29] M. Stratakis, H. Garcia, Catalysis by supported gold nanoparticles: beyond aerobic oxidative processes, *Chem. Rev.* 112 (2012) 4469–4506.
- [30] K. Cheng, M. Virginie, V.V. Ordonsky, C. Cordier, P.A. Chernavskii, M.I. Ivantsov, S. Paul, Y. Wang, A.Y. Khodakov, Pore size effects in high-temperature Fischer-tropsch synthesis over supported iron catalysts, *J. Catal.* 328 (2015) 139–150.
- [31] B. Zhang, X. Guo, H. Liang, H. Ge, X. Gu, S. Chen, H. Yang, Y. Qin, Tailoring Pt-Fe₂O₃ interfaces for selective reductive coupling reaction to synthesize imine, *ACS Catal.* 6 (2016) 6560–6566.
- [32] L. Wang, J. Zhang, Y. Zhu, S. Xu, C. Wang, C. Bian, X. Meng, F.S. Xiao, Strong metal-support interactions achieved by hydroxide-to-oxide support transformation for preparation of sinter-resistant gold nanoparticle catalysts, *ACS Catal.* 7 (2017) 7461–7465.
- [33] X. Qiao, L. Niu, H. Zhang, X. Wen, Y. Cao, G. Bai, Controllable fabrication of a novel porous Ni-alginate hybrid material for hydrogenation, *Appl. Catal. B: Environ.* 218 (2017) 721–730.
- [34] Z. Kónya, V.F. Puentes, I. Kiricsi, J. Zhu, J.W. Ager, M.K. Ko, H. Frei, P. Alivisatos, G.A. Somorjai, Synthetic insertion of gold nanoparticles into mesoporous silica, *Chem. Mater.* 15 (2003) 1242–1248.
- [35] Z. Jin, M. Xiao, Z. Bao, P. Wang, J. Wang, A general approach to mesoporous metal oxide microspheres loaded with noble metal nanoparticles, *Angew. Chem. Int. Ed.* 51 (2012) 6406–6410.
- [36] S. Saha, A. Pal, S. Kundu, S. Basu, T. Pal, Photochemical green synthesis of calcium alginate-stabilized Ag and Au nanoparticles and their catalytic application to 4-nitrophenol reduction, *Langmuir* 26 (2010) 2885–2893.
- [37] S.B. Hammouda, F. Fourcade, A. Assadi, I. Soutrel, N. Adhoum, A. Amrane, L. Monser, Effective heterogeneous electro-fenton process for the degradation of a malodorous compound, indole using iron loaded alginate beads as a reusable catalyst, *Appl. Catal. B: Environ.* 182 (2016) 47–58.
- [38] Y. Yan, K. Li, L. Thia, Y. Dai, J. Zhao, X. Chen, Y. Yang, J.M. Lee, Hydrothermally driven three-dimensional evolution of mesoporous hierarchical europium oxide hydrangea microspheres for non-enzymatic sensors of hydrogen peroxide detection, *Environ. Sci. Nano* 3 (2016) 701–706.
- [39] L. Shen, X. Zhang, E. Uchaker, C. Yuan, G. Cao, Li₄Ti₅O₁₂ nanoparticles embedded in a mesoporous carbon matrix as a superior anode material for high rate lithium ion batteries, *Adv. Energy Mater.* 2 (2012) 691–698.
- [40] X.L. Wu, W. Wang, Y.G. Guo, L.J. Wan, Template-free synthesis and super-capacitance performance of a hierarchically porous oxygen-enriched carbon material, *J. Nanosci. Nanotechnol.* 11 (2011) 1897–1904.
- [41] Z. Schneppe, S.C. Wimbush, S. Mann, S.R. Hall, Alginate-mediated routes to the selective synthesis of complex metal oxide nanostructures, *CrystEngComm* 12 (2010) 1410–1415.
- [42] Z. Schneppe, S.R. Hall, M.J. Hollamby, S. Mann, A flexible one-pot route to metal/metal oxide nanocomposites, *Green Chem.* 13 (2011) 272–275.
- [43] L. Ai, H. Yue, J. Jiang, Environmentally friendly light-driven synthesis of Ag nanoparticles in situ grown on magnetically separable biohydrogels as highly active and recyclable catalysts for 4-nitrophenol reduction, *J. Mater. Chem.* 22 (2012) 23447–23453.
- [44] S. Zhang, Q. Fan, H. Gao, Y. Huang, X. Liu, J. Li, X. Xu, X. Wang, Formation of Fe₃O₄/MnO₂ ball-in-ball hollow spheres as a high performance catalyst with enhanced catalytic performances, *J. Mater. Chem. A* 4 (2016) 1414–1422.
- [45] B. Mile, D. Stirling, M.A. Zammitt, A. Lovell, M. Webb, The location of nickel oxide and nickel in silica-supported catalysts: two forms of “NiO” and the assignment of temperature-programmed reduction profiles, *J. Catal.* 114 (1988) 217–229.
- [46] C. Zhao, Y. Yu, A. Jentys, J.A. Lercher, Understanding the impact of aluminum oxide binder on Ni/HZSM-5 for phenol hydrodeoxygenation, *Appl. Catal. B: Environ.* 132–133 (2013) 282–292.
- [47] J. Liu, C. Li, F. Wang, S. He, H. Chen, Y. Zhao, M. Wei, D.G. Evans, X. Duan, Enhanced low-temperature activity of CO₂ methanation over highly-dispersed Ni/TiO₂ catalyst, *Catal. Sci. Technol.* 3 (2013) 2627–2633.

- [48] T. Wang, H. Ma, L. Zeng, D. Li, H. Tian, S. Xiao, J. Gong, Highly loaded Ni-based catalysts for low temperature ethanol steam reforming, *Nanoscale* 8 (2016) 10177–10187.
- [49] H.P. Ren, Y.H. Song, Q.Q. Hao, Z.W. Liu, W. Wang, J.G. Chen, J. Jiang, Z.T. Liu, Z. Hao, J. Lu, Highly active and stable Ni-SiO₂ prepared by a complex-decomposition method for pressurized carbon dioxide reforming of methane, *Ind. Eng. Chem. Res.* 53 (2014) 19077–19086.
- [50] Z. Liu, J. Zhou, K. Cao, W. Yang, H. Gao, Y. Wang, H. Li, Highly dispersed nickel loaded on mesoporous silica: one-spot synthesis strategy and high performance as catalysts for methane reforming with carbon dioxide, *Appl. Catal. B: Environ.* 125 (2012) 324–330.
- [51] M. Bejblová, P. Zámotný, L. Červený, J. Čejka, Hydrodeoxygenation of benzophenone on Pd catalysts, *Appl. Catal. A Gen.* 296 (2005) 169–175.
- [52] J. Huang, Y. Jiang, N. van Vegten, M. Hunger, A. Baiker, Tuning the support acidity of flame-made Pd/SiO₂-Al₂O₃ catalysts for chemoselective hydrogenation, *J. Catal.* 281 (2011) 352–360.